Light Metals 2014
Edited by: John Grandfield
TMS (The Minerals, Metals & Materials Society), 2014

Light Metals 2014

ALUMINUM REDUCTION TECHNOLOGY

Fundamentals – Modeling

SESSION CHAIR
Martin Desilets
Sherbrooke University
Sherbrooke, QC, Canada

Light Metals 2014
Edited by: John Grandfield
TMS (The Minerals, Metals & Materials Society), 2014

ON THE PREDICTION OF THE CRUST EVOLUTION INSIDE ALUMINUM ELECTROLYSIS CELLS

Marc LeBreux[1], Martin Désilets[1], Alexandre Blais[2], Marcel Lacroix[1]
[1] Université de Sherbrooke, Sherbrooke (Québec) Canada J1K 2R1
[2] CRDA, RioTinto Alcan, Jonquière (Québec) Canada G7S 4K8

Keywords: Crust formation, Anode cover material, Numerical modeling, Heat transfer, Chemical reaction

Abstract

A model for predicting the evolution of the crust inside aluminum electrolysis cells is presented. The model takes into account the effects of heat transfer, solid/liquid phase-change, and chemical transformation of anode covering material (ACM). The model predicts: 1) the temperature field inside the cell, 2) the evolution of the ACM conversion into crust, 3) the melting/solidification processes inside the cell and, 4) the time-varying heat losses at the top of the cell. The model is validated with experimental data taken on an industrial electrolysis cell. Results show that the model captures the essential behavioral features of the industrial cell. However, further experiments must be performed in order to provide reliable data on the crust formation. These experimental data are needed for a thorough validation of the mathematical model.

Nomenclature

A	frequency factor (s^{-1})
A_s	cross section (m^2)
C_A	concentration of reactant A (mol/L)
C_p	specific heat (J/kg.K)
dt	time step (s)
dx,dy	mesh size (m)
E_a	activation energy (J/mol)
f	liquid fraction
h	heat transfer coefficient ($W/m^2.K$)
I	current (A)
k	thermal conductivity (W/m.K)
k_A	rate coefficient of the reaction A→B (s^{-1})
N_A	number of moles of reactant A (mol)
$\dot{q}$	volumetric heat generation (W/m^3)
q''	heat flux (W/m^2)
R	universal gas constant (J/mol.K)
t	time (s)
T	temperature (K)
X	conversion
δH	volumetric enthalpy change (J/m^3)
λ	heat of fusion (J/kg)
ρ	density (kg/m^3)
ρ_Ω	electrical resistivity (Ω.m)

Introduction

When the anode is changed in an aluminum electrolysis cell (Figure 1), operators cover the newly set anode with a cover material (Anode Cover Material). This material, made of alumina and recycled crushed bath, is used to prevent anode air burn, to control the heat losses at the top of the cell, and to minimize the fluoride fumes emissions.

While the cell is in operation, part of the ACM transforms itself from a granular material into a solid and dense crust. It is generally accepted that the crusting behavior of the ACM starts with the conversion of alumina transition phases to alpha platelets and continues by the consolidation or 'gluing' of the bath particles [1,2].

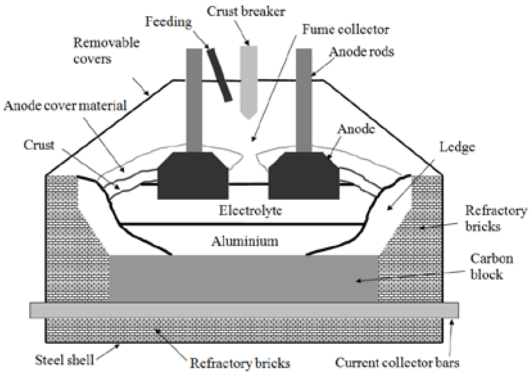

Figure 1. Schematic of an aluminum electrolysis cell

The majority of the studies dedicated to the crust formation are experimental [3,4]. Only a handful of investigations have focused on crust formation inside industrial electrolysis cells [2,5]. Liu et al. showed that the ACM composed of both alumina and recycled crushed bath has a high thermal conductivity. As a result, it releases more heat than electrolysis cells containing alumina only. Also, their study showed that a smaller cavity is created underneath high thermal conductivity crust during the operation of the cell.

In the past, a lot of efforts have been devoted to the mechanism of crust formation using alumina based ACM [4,6,7]. However, during the last 20 years, the standard ACM mixture used in prebake aluminum smelters has been composed of alumina and crushed bath. Nowadays, the studies of crust formation are thus conducted with the standard ACM [1,2,5,8,9]. For example, the thermal properties of the ACM and of the crust were investigated in Refs. [8,9]. These studies showed that the ACM granulometry has a greater impact on its thermal conductivity than the composition of the ACM itself, and that the properties of the ACM are closely related to the cell top heat losses. However, the majority of the proposed heat transfer models for predicting the heat losses are limited to the one dimensional steady-state analyses [9-12]. These models ignore the multi-dimensional dynamic processes that govern the crust evolution.

This paper remedies these shortcomings by presenting a two-dimensional model for predicting the evolution of the crust inside aluminum electrolysis cells.

Numerical model

The process of crust evolution is depicted in Figure 2. At time t=0, the ACM is deposited on top of the newly set anode (Figure 2a). Due to the cell's heat load, the ACM heats up and then starts transforming itself from a granular material into a solidified dense

crust (Figure 2b). As the cell continues to dissipate heat, the newly formed crust can melt in the regions where the temperature exceeds that of its liquidus. As a result, a cavity may form underneath the crust (Figure 2 c). In order to predict the formation and evolution of the crust inside aluminum electrolysis cells, the proposed numerical model takes into account the simultaneous processes of heat transfer, chemical reaction and phase-change.

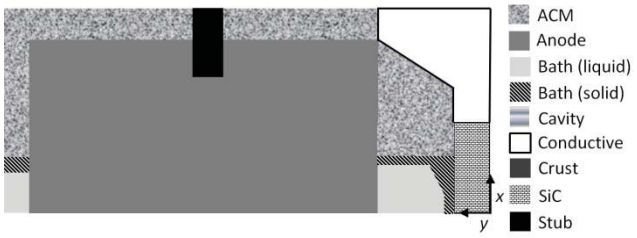

a) At time $t = 0$, the ACM is deposited

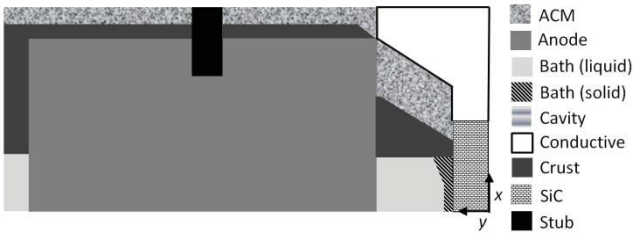

b) At time $t > 0$, the ACM transforms into a solid crust

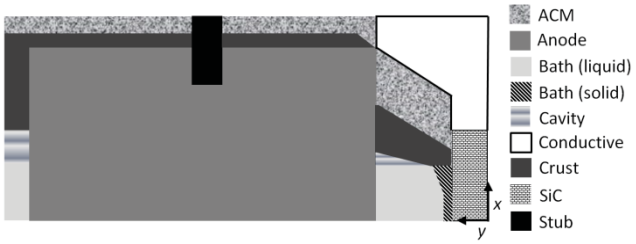

c) At time $t >> 0$, the crust melts and a cavity is formed

Figure 2. Schematic of the numerical model

The following assumptions are retained:

- The crust formation is controlled by heat transfer processes [6,9].
- The phase change problem is non-isothermal. It is characterized by a mushy zone separating the solidus temperature $T_{solidus}$ from the liquidus temperature $T_{liquidus}$.
- The ACM granulometry is similar to the coarse crushed bath mixture presented in Ref. [9]. Its characteristic thermal conductivity is adopted.
- The thermo physical properties of all the materials illustrated in Figure 2 are known.
- The thermo physical properties of the ACM depend on the conversion as the material transforms itself into a solid crust.
- The heat transfer across the liquid bath layer is convection dominated. The effect of the flow circulation into the liquid layer is accounted for by means of an 'augmented effective' thermal conductivity.
- The anode height remains constant. Its consumption is ignored.
- The thermo electric Joule effect that stems from the current flow through the anode and the stub is set equal to $\dot{q} = \rho_\Omega (I/A_s)^2$.

Based on the foregoing assumptions, the governing phase change heat diffusion equation for each of the materials is stated as:

$$\rho C_p \frac{\partial T}{\partial t} = \nabla(k\nabla T) + \dot{q} - \delta H \frac{\partial f}{\partial t} \quad (1)$$

The conditions for the boundaries identified in Figure 3 are summarized in Table I. The initial conditions are the following:

$$T(x, y, t = 0) = T_0(x, y) \quad (2)$$

$$f(x, y, t = 0) = f_0(x, y) \quad (3)$$

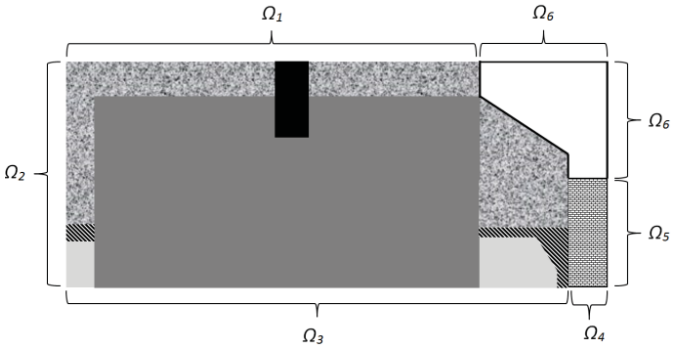

Figure 3. Boundaries of the numerical model

Table I. Boundary conditions of the numerical model [9,13]

Boundary	Condition
Ω_1	Convection (h=70 W/m^{2}K, T_∞=125 degC)
Ω_2	Symmetry
Ω_3	Specified temperature (T_{bath} =960 degC)
Ω_4	Insulated
Ω_5	Convection (h=30 W/m^{2}K, T_∞=30 degC)
Ω_6	Convection (h=100 W/m^{2}K, T_∞=125 degC)

The enthalpy change is defined as $\delta H = \rho(C_{p,liquid} - C_{p,solid})T + \rho\lambda$. The liquid fraction f varies linearly between the solidus temperature $T_{solidus}$ and the liquidus temperature $T_{liquidus}$ in the following manner:

$$f = f(T) = \begin{cases} 0 & T \le T_{sol} \\ \left(\frac{T - T_{sol}}{T_{liq} - T_{sol}}\right) & T_{sol} < T < T_{liq} \\ 1 & T \ge T_{liq} \end{cases} \quad (4)$$

Eqs. (1-4) were discretized using second-order finite differences in space and a first-order difference in time with an implicit scheme. As a compromise between accuracy and CPU time requirements, the mesh size was set equal to dx=dy=0.01 m and the time step, dt=200 s. The resulting set of algebraic equations was solved using the iterative Gauss-Seidel algorithm, thus providing the temperature field $T(x,y)$ at each time step. The liquid fraction f in Eq. (1) was determined according to the enthalpy method developed by Voller and Swaminathan [14].

In order to represent the transformation of the granular ACM into a solid crust, a simplified chemical reaction model is considered:

$$A \rightarrow B \quad (5)$$
$$\text{ACM} \rightarrow \text{crust}$$

For a pseudo-first order reaction, the rate of transformation of the ACM is defined as:

$$\frac{dC_A}{dt} = -k_A C_A \quad (6)$$

Using an Arrhenius model to represent the influence of temperature, one gets:

$$k_A = A \exp\left(-E_a/RT\right) \quad (7)$$

The temperature T is provided by the solutions of Eqs 1-4.

Knowing that $C_A = \frac{N_A}{V}$ and $N_A = N_{A0}(1 - X)$, the conversion X varies with time and temperature according to

$$X = (X_0 - 1) \exp(-k_A t) + 1 \quad (8)$$

The conversion X is a number between 0 and 1. It represents the degree of transformation of the ACM into crust at time t and position x and y. A value of X=0 means that the ACM remains as the original granular material deposited during the anode change procedure. On the other hand, when X=1 the ACM has fully transformed itself into a solid crust. During the course of the reaction, the ACM thermo physical properties $\alpha\ (\rho, k, C_p, \lambda)$ vary with the conversion (Eq.9):

.

$$\alpha_{ACM \rightarrow crust} = (1 - X)\ \alpha_{ACM} + X\ \alpha_{crust} \quad (9)$$

The solution of Eqs. 1-9 provides the following information:

1- The temperature field *T(x,y,t)*
2- The ACM conversion into crust *X(x,y,t,T)*
3- The liquid fraction field *f(x,y,t)*
4- The heat flux distribution *q''(x,y,t)*

The conversion enables to predict the crust top position inside the cell. The crust bottom position is given by the liquid fraction that explains the liquefaction of the crust once it is formed. As for the heat flux distribution, it enables the calculation of the specific components of the cell top heat losses.

The usefulness of the proposed numerical model is exemplified in the following example. The predicted initial and steady-state isotherms are shown in Figure 4. The initial isotherms were obtained with the model by simulating the waiting time, typically 4 hours, between the setting of a new anode and the moment when the ACM is deposited. The waiting time is necessary in order to solidify the top of the bath where the ACM is deposited. At steady-state and for the zone that extends from the anode to the sidewall (ASD), the heat transfer is truly two-dimensional. The isotherms of the ACM are oblique. In the other zones however, where the ACM was deposited, the heat transfer remains one-dimensional. The isotherm lines are horizontal.

Table II. Thermophysical properties of the materials [6,8,9,15]

Thermophysical properties	**Value**
$k_{bath,solid}$ (W/m.K)	1
$k_{bath,liquid}$ (W/m.K)	100 (augmented)
k_{ACM} (W/m.K)	0.27+0.000913*T
$k_{crust,solid} = k_{crust,liquid}$ (W/m.K)	1.6
k_{SiC} (W/m.K)	Confidential
k_{anode} (W/m.K)	-0.000003*T^2 + 0.0056*T + 3.4
k_{stub} (W/m.K)	Confidential
$C_{p,bath,solid} = C_{p,bath,liquid}$ (J/kg.K)	1800
$C_{p,ACM}$ (J/kg.K)	1200
$C_{p,crust,solid} = C_{p,crust,liquid}$ (J/kg.K)	1500
$C_{p,SiC}$ (J/kg.K)	Confidential
$C_{p,anode}$ (J/kg.K)	1050
$C_{p,stub}$ (J/kg.K)	Confidential
$\rho_{bath,solid} = \rho_{bath,liquid}$ (kg/m^3)	2100
ρ_{ACM} (kg/m^3)	1500
$\rho_{crust,solid} = \rho_{crust,liquid}$ (kg/m^3)	2600
ρ_{SiC} (kg/m^3)	Confidential
ρ_{anode} (kg/m^3)	1560
ρ_{stub} (kg/m^3)	Confidential
λ_{bath} (J/kg)	510000
λ_{crust} (J/kg)	200000
$\lambda_{SiC} = \lambda_{ACM} = \lambda_{anode} = \lambda_{stub}$ (J/kg)	0
$T_{solidus,bath}$ (degC)	900
$T_{liquidus,bath}$ (degC)	950
$T_{solidus,crust}$ (degC)	700
$T_{liquidus,crust}$ (degC)	900
$\rho_{\Omega,anode}$ (μΩ.m)	0.0121*T + 60
$\rho_{\Omega,stub}$ (μΩ.m)	Confidential

Table III. Arrhenius model parameters

Parameters	**Value**
E_a (J/mol)	135000
A (s^{-1})	1000

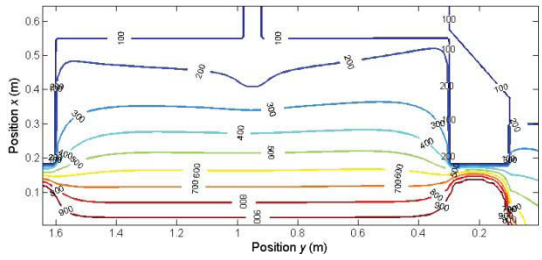

a) Initial

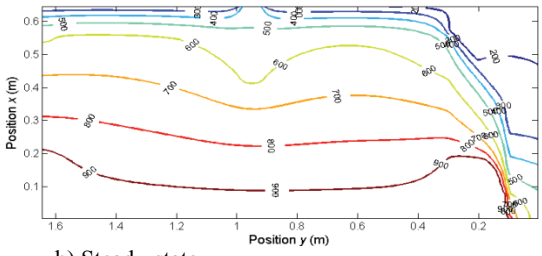

b) Steady-state

Figure 4. Isotherms (degC) predicted by the numerical model

Similar conclusions may be drawn by examining the steady-state conversion field shown in Figure 5. Once again, the conversion enables the prediction of the crust top position inside the electrolysis cell. Due to the facts that (1) less ACM is deposited on the top of the anode and (2) the heat load from the bath has less influence at this position, the crust is thinner. Moreover, the crust is thicker on the left side of the anode. In this region, the bath is insulated whereas on the right side it is cooled by convection.

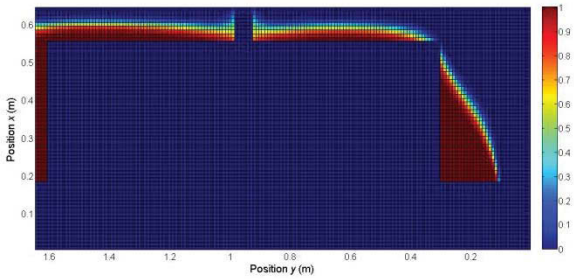

Figure 5. Steady-State conversion predicted by the numerical model

The initial and steady-state liquid fraction fields are illustrated in Figure 6. For a liquid fraction of 0 (blue), the material is solid. For a liquid fraction of 1 (red), the material is completely melted. Figure 6 a) shows that at the initial time, the liquid bath has solidified into a ledge on the wall. Moreover, a frozen layer prevails on the top of the bath. Figure 6 b) shows that the frozen layer and the bottom of the crust have melted. In this case, a cavity between the bath surface and the bottom of the crust was created.

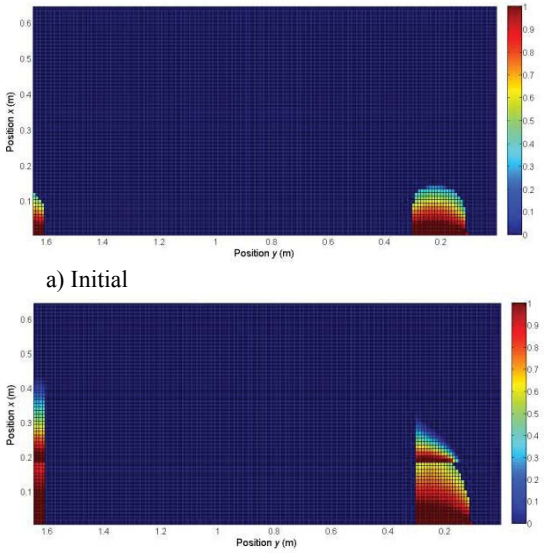

a) Initial

b) Steady-state

Figure 6. Liquid fraction field predicted by the numerical model

Experimental data

The mathematical model was validated with experimental data taken on an industrial aluminum electrolysis cell. The experimental tests were carried out on a P155 prebake cell at RioTinto Alcan's Grande-Baie plant located in Québec, Canada. Once the newly set anode was installed, 6 type K thermocouples (inconel sheath, diameter of 1/8'') were installed in the cell (Figure 7). Each thermocouple (TC) is located at the center of the ASD, but at different heights. The thermocouples are spaced 6 cm apart vertically with TC #6 being located on the top of the ACM.

Figure 7. Thermocouples assembly inside the industrial electrolysis cell

In order to monitor the temperature continuously during the course of the experiment, the thermocouples were connected to a Hioki portable data acquisition system. Once the temperature readings were available, the ACM was deposited gently inside the cell. The ACM available at the plant had a typical composition [9] while the ACM granulometry was analysed at the CRDA laboratory. Results showed that the ACM granulometry was similar to that of the coarse crushed bath (CCB) reported in Ref. [9].

Figure 8 compares the predicted and measured temperatures at the ASD center for different heights.

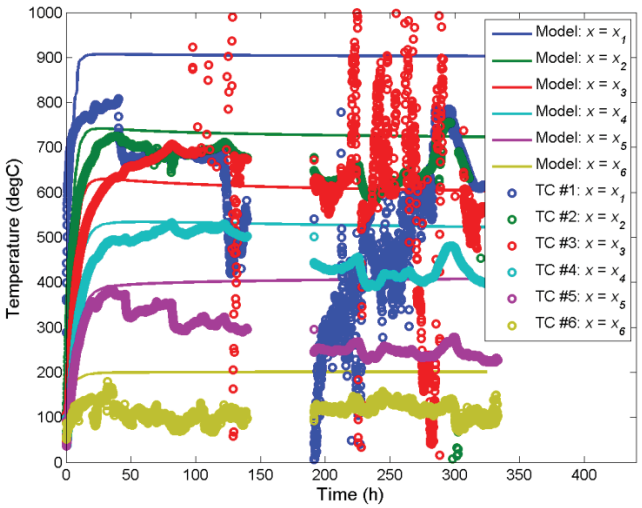

Figure 8. Comparison between the predicted and measured temperatures at the ASD center for different heights

It is seen that the measured temperature on the top of the ACM (TC #6) is lower than the predicted temperature. It indicates that convection cooling at the top of the ACM was underestimated.

However, previous measurements done at Grande-Baie plant showed that the ACM top temperature may vary between 180-210 degC. This suggests that more measurements are needed in order to confirm the ACM top temperature.

Figure 8 also shows that the predicted and the measured temperatures at heights $x=x_2$, $x=x_4$ and $x=x_5$ are in fairly good agreement during the first 50 hours. However, the temperatures measured by TC #3 located at $x=x_3$ are larger than that predicted by the numerical model. It is suspected that the thermal conductivity of the crust was underestimated in the model. On the other hand, the temperatures measured by TC #1 are lower than the predictions. In this case, it appears that the bath heat load was overestimated in the numerical model.

Moreover, looking at the temperature measurements, one can perceive the effect of metal siphoning performed on the cell at time t = 50 h, t = 90 h and t = 225 h. In both cases, the thermocouples recorded temperature drops between 50 and 100 degC. Figure 8 also shows that the Hioki was accidentally shut off from time t = 150 h to t = 200 h, and thus no temperature measurements were available for that period of time. Finally, Figure 8 shows that at heights $x=x_2$, $x=x_3$ and $x=x_4$, the temperatures predicted by the numerical model decrease as time passes. As more conductive crust replaces the insulating ACM, it is possible to lower the thermal resistance of the system thereby decreasing the temperature at these positions. This trend was also recorded by the thermocouple assembly.

Other manual measurements such as the top crust temperature and the crust thickness were taken at the center of the ASD. The top crust temperature was obtained by inserting a thermocouple into the ACM cover until it hits the surface of the solid crust, i.e. the crust top position. The thermocouple was connected to a hand-held Fluke multi meter providing the top crust temperature measurement. Figure 9 compares the predicted and the measured top crust temperatures.

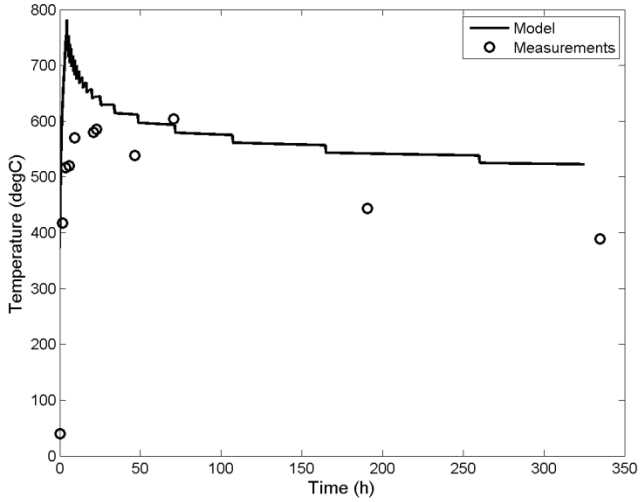

Figure 9. Comparison between the predicted and measured top crust temperature at the center of the ASD

It is seen that the crust temperature decreases with time. Furthermore, the numerical model overestimates the temperatures at the beginning of the experiment and for time t > 100 h. This is due to the fact that the crust thickness was underestimated in the model.

The crust thickness is defined by the top and bottom positions of the crust. The crust top position was determined by first measuring the thickness of the deposited ACM. Afterwards, as the crust grew, the remaining thickness of the ACM was measured with a ruler and thus the crust top position could be deduced. As for the crust bottom position, it corresponds to the height of the cavity between the bath surface and the bottom of the crust. During the measurements campaign, such a data was not available. However, past measurements done at RioTinto Alcan plant of Grande-Baie showed that the height of the cavity varied from 0.01m to 0.11 m near the center of the ASD. Figure 10 compares the predicted and the measured crust positions.

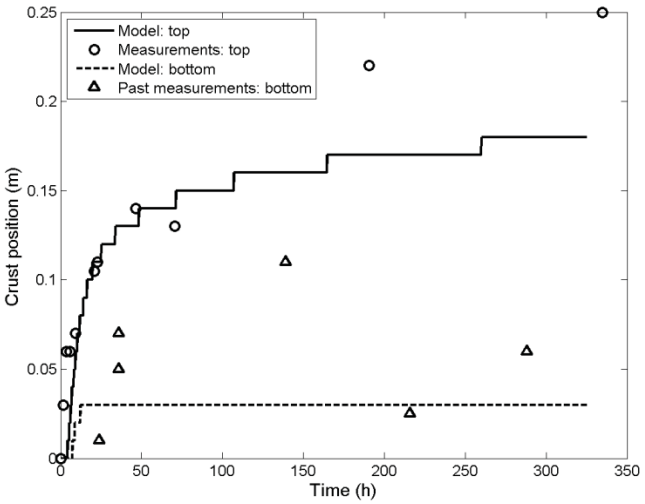

Figure 10. Comparison between the predicted and measured crust positions at the center of the ASD

This figure shows good agreement between the measured and predicted crust top position during the first 100 hours. However, from time t=200 h until the end of the experiment, the measurements of the top position exceeded the predictions. Again, this is due to the difficulties of locating the top surface of the crust inside the industrial cell.

As for the crust bottom position, measurements showed that the height of the cavity were larger than the predictions of the model. Thus, in that case, the crust is thinner. Since they were taken on different cells, one can also note the presence of variability in the measurements. Moreover, Figure 10 show that the steady-state regime for the crust bottom position was attained much faster with the numerical model than with the measurements. Additional measurements of both the top and bottom positions of the crust are thus necessary in order to confirm the process of crust evolution.

Finally, since no heat flux sensors were available during the measurement campaign, it was not possible to estimate the cell top heat losses. These losses may however be estimated with the one-dimensional Fourier's law:

$$q''(x) = \frac{k_{ACM}(T)\,\Delta T}{\Delta x} \qquad (10)$$

Figure 11 compares the predicted and estimated (Eq. 10) heat fluxes. The agreement between both is relatively good at the start of the experiment. Moreover, these results agree with the heat flux of ≈ 2000 W/m^2 measured on the top of the ACM and reported in Ref. [2,9]. However, the predictions of the heat fluxes close to the bath (height x=(x_1+x_2)/2), between time t=50 h and t=125 h are much higher than the estimated values from Eq. 10, i.e., 5500 W/m^2 compared to 500-1000 W/m^2. This suggests that the bath heat load was overestimated in the numerical model.

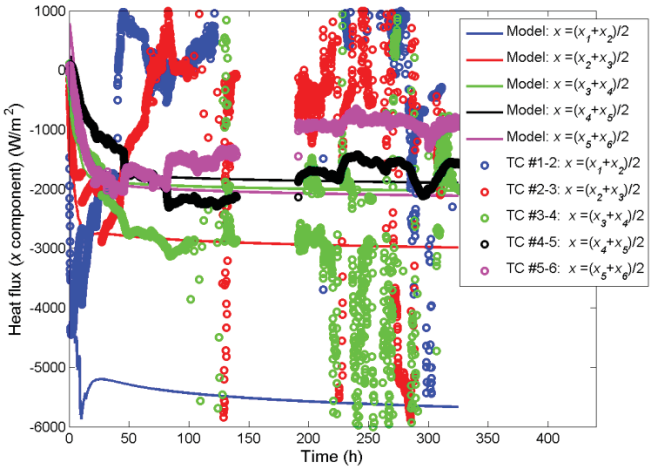

Figure 11. Comparison between the predicted and measured heat fluxes (x component) at the ASD center for different heights

Concluding remarks

A model for predicting the evolution of the crust inside aluminum electrolysis cells was presented. The model integrates processes that involve heat transfer, solid/liquid phase-change, and chemical reactions. The model predicts: 1) the temperature field, 2) the ACM conversion field, 3) the liquid fraction field, and 4) the heat flux distribution in the top region of the cell. The model was validated with experimental data collected on an industrial electrolysis cell. Results showed that the predictions capture the essential behavioral features of the industrial cell.

The proposed model is still under development. More measurements from industrial cells are needed for its improvement. A second measurement campaign is already planned.

Acknowledgments

The authors are very grateful to the Natural Sciences and Engineering Research Council of Canada (NSERC) and RioTinto Alcan for their financial support. The authors would also like to thank the CRDA reduction technician's team and the personnel of Usine Grande-Baie for their valuable help during the course of the measurement campaign.

References

[1] Q. Zhang, M.P. Taylor, J.J.J. Chen, D. Cotton, T. Groutzo, X. Yang, Composition and Thermal Analysis of Crust Formed from Industrial Anode Cover, TMS Light Metals, 2013, pp. 675-680.
[2] X. Liu, M.P. Taylor, S.F. George, Crust Formation and Deterioration in Industrial Cells, TMS Light Metals, 1992, pp. 489-494.
[3] T.J. Johnston, N.E. Richards, Correlation between alumina properties and crust, TMS Light Metals, 1983, pp. 623-639.
[4] T. Eggen, S. Rolseth, K.A. Rye and J. Thonstad, Alumina Crusting in Cryolite Melts - Part I: Penetration of Molten Electrolyte into Alumina, TMS Light Metals, 1992, pp. 495-502.
[5] T. Groutso, M.P. Taylor, A.K. Hudson, Aspects of Crust Formation from Today's Anode Cover Material, TMS Light Metals, 2009, pp. 405-410.
[6] K.A. Rye, Crust formation in cryolite based baths, Ph.D thesis, Technical University of Norway, Trondheim, 1992.
[7] A.J. Becker, T.R. Hornack, T.J. Steinbeck, In-situ Properties of Crust Formed with Five Ores in a Soderberg Smelting Cell, TMS Light Metals, 1987, pp. 41-50.
[8] H. Wijayaratne, M. Hyland, M.P. Taylor, A. Grama, T. Groutso, Effects of Composition and Granulometry on Thermal Conductivity of Anode Cover Materials, TMS Light Metals, 2011, pp. 399-404.
[9] S. Xianchun, Top Cover and Energy Balance in Hall-Héroult Cells, Ph.D thesis, University of Auckland, 2006.
[10] M.D. Gadd, B.J. Welch, A.D. Ackland, The Effect of Process Operations on Smelter Cell Top Heat Losses, TMS Light Metals, 2000, pp. 231-237.
[11] K.A. Rye, J. Thonstad, X. Liu, Heat Transfer, Thermal Conductivity, and Emissivity of Hall-Héroult Top Crust, TMS Light Metals, 1995, pp. 441-449.
[12] M.P. Taylor, G.L. Johnson, E.W. Andrews, B.J. Welch, The Impact of Anode Cover Control and Anode Assembly Design on Reduction Cell Performance,TMS Light Metals, 2004, pp. 199-206.
[13] F.P. Incropera, D.P. DeWitt, Fundamentals of Heat and Mass Transfer, fifth ed., John Wiley & Sons, 2002.
[14] V.R. Voller, C.R. Swaminathan, General Source-Based Method for Solidification Phase Change, Numerical Heat Transfer part B 19 (1991) 175-189.
[15] C.C. Wei, J.J.J. Chen, B.J. Welch, V.R. Voller, Modeling of Dynamic Ledge Heat Transfer, TMS Light Metals, 1997, pp. 309-316.